Breton Florentin (Orcid ID: 0000-0002-5982-8182)
Vrac Mathieu (Orcid ID: 0000-0002-6176-0439)
Vaittinada Ayar Pradeebane (Orcid ID: 0000-0001-8085-9621)
Jézéquel Aglaé (Orcid ID: 0000-0002-0957-3126)

Seasonal circulation regimes in the North Atlantic: towards a new seasonality

Florentin Breton[1,2*], Mathieu Vrac[1†], Pascal Yiou[1‡], Pradeebane Vaittinada Ayar[3,4‡] and Aglaé Jézéquel[5‡]

Author affiliations:
[1] Laboratoire des Sciences du Climat et de l'Environnement, UMR8212 CEA – CNRS – UVSQ, Université Paris-Saclay and IPSL, Orme des Merisiers, Gif-sur-Yvette, France
[2] Laboratoire Image Ville Environnement, UMR 7362, CNRS/UDS, Strasbourg, France
[3] Institut National de la Recherche Scientifique | INRS · Eau Terre Environnement Centre, Québec, Canada.
[4] NORCE Norwegian Research Centre AS, Bjerknes Centre for Climate Research, Bergen, Norway
[5] LMD/IPSL, Ecole Normale Supérieure, PSL research University, Paris, France

Author contributions:
*Design of the research, gathering of the data, analysis, interpretation and discussion of findings, drafting the article, article revision.
†Design of the research, interpretation and discussion of findings, drafting the article, article revision.
‡Interpretation and discussion of findings, article revision.

Correspondence: florentin.breton@live-cnrs.unistra.fr and mathieu.vrac@lsce.ipsl.fr

Funding information:
The authors acknowledge financial support from the CoCliServ and EUPHEME projects that are part of ERA4CS, an ERA-NET initiated by JPI Climate and co-funded by the European Union.

Abstract:

European climate variability is shaped by atmospheric dynamics over the North Atlantic and local processes. Better understanding their future seasonality is essential to anticipate changes in weather conditions for human and natural

This article has been accepted for publication and undergone full peer review but has not been through the copyediting, typesetting, pagination and proofreading process which may lead to differences between this version and the Version of Record. Please cite this article as doi: 10.1002/joc.7565

systems. We explore atmospheric seasonality over 1979- 2017 and 1979-2100 with seasonal circulation regimes (SCRs), by clustering year-round daily fields of Z500 from the ERA-Interim reanalysis and 12 CMIP5 climate models (historical and RCP8.5 runs). The spatial and temporal variability of SCR structures and associated patterns of surface air temperature are investigated. Climate models have biases but reproduce structures and evolutions of SCRs similar to the reanalysis over 1979-2017: decreasing frequency of winter conditions (starting later and ending earlier in the year) and the opposite for summer conditions. These changes are stronger over 1979-2100 than over 1979-2017, associated with a large increase of North Atlantic seasonal mean Z500 and temperature. When using more SCRs (more freedom in definition of seasonality), the changes over 1979-2100 correspond to a long-term swap between SCRs, resulting in similar structures (annual cycle and spatial patterns) relative to the evolution of seasonal mean Z500 and temperature.
To understand whether the evolution of SCRs is linked to uniform warming, or to changes in circulation patterns, we remove the calendar trend in the Z500 regional average to define SCRs based on detrended data (d-SCRs). The temporal properties of d-SCRs appear almost constant whereas their spatial patterns change, indicating that the calendar Z500 regional trend drives the evolutions of SCRs, and that changing spatial patterns in d-SCRs account for the heterogeneity of this trend. Our study suggests that historical winter conditions will continue to decrease in the future while historical summer conditions continue to increase. However, it also suggests that the spatial and temporal patterns of SCRs would remain similar, relatively to the year-round Z500 increase.

Keywords:
Seasonality, atmospheric circulation, North Atlantic, surface temperature, spatial patterns, annual cycle, past, future

1 | Introduction

Are seasons changing? If so, are those changes due to climate change or to natural variability? It appears that the answers might strongly depend on the definition of season. Indeed, many investigations of seasonality have been carried out based on different definitions of the seasons (see literature reviews in IPCC (2013); Hoegh-Guldberg et al. (2018); Jia et al. (2019)). These investigations found changes both regarding variables in climatological seasons (e.g. decreasing winter and spring frost, decreasing summer Arctic sea ice) and regarding the seasonality of variables themselves (e.g. longer growing season, longer fire weather season). The meteorological seasons are a prominent feature of climate variability, experienced by human systems (e.g. health, transportation, energy) and natural systems (e.g. phenology) through the seasonality of surface weather conditions. In Europe, these conditions mostly result from the combined effects of large-scale circulation dynamics over the North Atlantic and local-scale processes that reduce or amplify

dynamic effects (Cattiaux, 2010). In this paper, we will define and investigate seasonality based on synoptic atmospheric circulation.

North Atlantic atmospheric patterns are the results of physical phenomena operating at different scales: “low-frequency” quasi-static structures such as the Icelandic Low and the Azores High (Angell & Korshover, 1974; Marshall et al., 2001; Wang, 2002; Hurrell & Deser, 2010) and “high-frequency” eddies or propagating synoptic waves such as cyclones and anticyclones (Price & Magaard, 1986; Barnston & Livezey, 1987) associated to the eddy-driven jet stream (Blackmon et al., 1984; Woollings et al., 2010; Franzke et al., 2011; Stendel et al., 2021). Due to these low-frequency and high-frequency components, the atmospheric dynamic variability of the North Atlantic is organized into preferential configurations (i.e. modes of variability) despite having a stochastic nature. One way to study these modes of variability or weather patterns is through weather regimes (WRs), defined as recurring atmospheric patterns (Vrac & Yiou, 2010; Hertig & Jacobeit, 2014). Since their first use in the middle of the XXth century in meteorology (Lamb, 1950; Rex, 1950), WRs have been reintroduced in the beginning of 1980s (e.g. Reinhold & Pierrehumbert (1982)) and largely used to better understand the variability of atmospheric dynamics (e.g. Vautard (1990)) and weather extremes (Hannachi et al., 2017), but also to evaluate climate models (Sanchez-Gomez et al., 2009; Díaz-Esteban et al., 2020; Fabiano et al., 2020). Extratropical climate variability is largely seasonally dependent (Wallace et al., 1993), and both climate dynamics (Woollings et al., 2010; Iqbal et al., 2018) and weather extremes (Cattiaux et al., 2012; Lhotka & Kysely, 2015; Brunner et al., 2018) have strong seasonal features. For instance, atmospheric blocking conditions facilitate cold spells in winter (Sillmann et al., 2011) and heatwaves in summer (Schaller et al., 2018). Furthermore, the seasonality of atmospheric dynamics has changed in the last decades with a lengthening of the period with summer conditions, starting earlier and ending later, and a shortening of the period with winter conditions (Vrac et al., 2014). When defining seasons based on the relationship between sea level pressure and surface air temperature, Cassou & Cattiaux (2016) found that the earliness of summer conditions should continue to increase in the future while no trend is found for winter conditions. One limitation is that these results strongly depend on the definition of the seasons and on the good representation of these seasons in the climate models. More generally, we have limited confidence in the representation of atmospheric circulation in models, and the confidence in the understanding of dynamic aspects of climate change is lower than for thermodynamic aspects (Shepherd, 2014). Therefore, it is essential to evaluate how models reproduce seasonality over a historical time period. This is a necessary step prior to investigating future seasonality changes based on a non-stationary definition of seasons.

In the present paper, we investigate synoptic climatological seasonality in the North Atlantic region through the use of “seasonal circulation regimes” (SCRs, as in Vrac et al. (2014)) that are defined by the probabilistic clustering of daily conditions of atmospheric circulation over a given time period without a priori separation of seasons. The evolution of circulation seasonality is then investigated through the

variability of SCRs (structures, trends). SCRs were developed to investigate non-stationary circulation seasonality through their ability to represent the evolution of atmospheric circulation modes (Vrac et al., 2007) with season-like behavior (Vrac et al., 2014). The planetary increase in geopotential height at 500 hPa (Z500) due to human influence is expected to drive SCR evolutions (Christidis & Stott, 2015). To test if SCR evolutions are driven by this increase, or by changes in spatial patterns of circulation, we also look at SCRs obtained from detrended geopotential height data. This investigation allows us to remove the effects of the North Atlantic increase in Z500 and therefore to disentangle the potential causes of the temporal and spatial SCR evolutions. The scientific objectives of the present study are to answer the following questions:

- How are climate models able to represent the past variability of seasonality over 1979-2017 with respect to reanalyses?
- What is the temporal and spatial evolution of seasonal structures over 1979-2100?
- What are the causes of seasonal evolutions?

The paper is organized as follows: Section 2 describes the reanalysis and climate model data used in this study, as well as the clustering method to define seasonal circulation regimes; Section 3 displays the results; and in Section 4, we discuss the findings and conclude.

2 | METHODS

2.1 | Data and preprocessing

We use daily average fields of geopotential height at 500 hPa (Z500) as a proxy of atmospheric circulation from the ERA-Interim (hereafter ERAI) reanalysis dataset (0.75° x 0.75° spatial resolution; Dee et al. (2011)) and simulations from 12 climate models of the Coupled Model Intercomparison Project fifth phase (CMIP5; Taylor et al. (2012)) over the North Atlantic region (22.5 to 70.5°N, 77.25°W to 37.5°E) from 1979 to 2017, and then from 1979 to 2100 (the datasets are briefly described in Table 1). The methodological choice of Z500 is motivated by its intermediate representation of atmospheric circulation between low- (weather systems) and high-level (jet-stream) dynamics, and its smoothness relative to other proxies of atmospheric circulation for facilitating the identification of the emergence (signal) of long-term changes in the climate system (e.g. sea level pressure is noisy). Daily average fields of surface air temperatures (TAS) from the same datasets are also extracted to study the temperature features of SCRs.

Raw year-round data is used rather than seasonal (e.g. summer or winter) data or deseasonalized anomalies to capture both the year-round seasonal cycle and any long-term trend. In order to make the analyses and comparisons easier, all datasets are first given the same format. Calendars are standardized to 365 days per year

ignoring bisextile years except for the Hadley Center simulations (year of 360 days). Historical experiment runs from climate models over 1979-2005 are concatenated to RCP8.5 experiment runs over 2006-2100 (respectively 1981-2005 and 2006-2099 for the Hadley Center model). The choice of the RCP8.5 scenario is motivated by its approximate representation of the current climate trajectory and its plausibility for future climate trajectory (Schwalm et al., 2020a,b), as well as its large magnitude of scenario forcing for facilitating the emergence of long-term changes in the climate system. The spatial grids of data from climate model simulations are bilinearly interpolated to the ERAI grid.

A principal component analysis (PCA) is applied to the regridded Z500 fields in order to reduce the dimension of the data while keeping most of the variability and seasonality. The raw Z500 data are scaled by the square root of the cosine of the latitude to give equivalent weight to all grid cells when performing the PCA (as in e.g. Cassou (2008)). Only the first principal component (PC1) is kept and used for clustering because it captures between about 49% and 60% of the variance and between about 95% and 99% of the annual cycle (spectral power at a frequency of 1/365 days; 1/360 days for the Hadley Center model) over 1979-2017 for ERAI (similar to Vrac et al. (2014) on another reanalysis) and all climate models (not shown). A large part of the long-term variability is also contained in PC1 (Figure S1), while the spatial pattern (eigenvectors) and statistical distribution (pdf) of PC1 are generally similar between ERAI and models over 1979-2017 (Figures S2-S3). Including more PCs in the analysis provided similar results (not shown) but brought more noise (more variance but only little more seasonality).

2.2 | Definition of seasonal circulation regimes

The definition of the SCRs is based on the classification of the PC1 time series into several groups (Gaussian-like distributions). We use the Expectation-Maximization (EM) algorithm (Dempster et al., 1977) based on a Gaussian mixture model (GMM; Peel & McLachlan (2000)) to classify probabilistically the 14235 days (13320 for the Hadley Center model) of the 1979-2017 period into SCRs. The EM algorithm estimates a multivariate probability density function (pdf) f of the data (here, daily PC1 values) as a weighted sum of K Gaussian pdfs f_k (k = *1, ..., K*) (Pearson, 1894):

$$f(x) = \sum_{k=1}^{K} \pi_k \, f_k \, (\, x \, ; \alpha_k \,)$$

where α_k contains the parameters (means μ_k and covariance matrix Σ_k) of f_k and $\pi_k$is the mixture ratio corresponding to the prior probability that x (i.e. PC1 value) belongs to f_k. The parameters α_k and π_k (k = *1, ..., K*) of the GMM are unknown and must be estimated (cf. Appendix). Finally, each cluster C_k of days is defined based on the Gaussian pdfs, according to the principle of posterior maximum:

$$C_k = \{ x ; \pi_k f_k (x ; \alpha_k) \geq \pi_j f_j (x ; \alpha_j) , \quad \forall j = 1, \ldots, K \}$$

In other words, each day is assigned to the cluster for which the probability of belonging is maximum, and the obtained clusters are SCRs which correspond to a classification of the daily data. The freedom of EM in the definition of the SCRs strongly depends on the number *K* of clusters and on the constraints applied to the covariance matrices (constraining the geometry of the clusters, cf. Appendix). We tried different values for K (from K = 1 to K = 15) and evaluated them through the Bayesian Information Criterion (BIC; Schwarz et al. (1978)). Optimizing the BIC achieves a compromise between overfitting the observations with the model and the complexity of the model (cf. Appendix). Four SCRs (hereafter SCR4) correspond both to a plateau of BIC (Figure A1 in Appendix) and to the traditional (astronomical) number of seasons, although SCR4 emphasizes winter and summer but downplays spring and autumn.

The GMM with the best BIC is selected. Different clustering methods can lead to different results (e.g. Philipp et al. (2010)) so we tested the sensitivity of the SCR results to using the k-means clustering algorithm (more popular but less flexible; Estivill-Castro and Yang (2000); Rokach & Maimon (2005); Han et al. (2011)) instead of EM, which brought very similar results (not shown). EM can be seen as a generalization of k-means with less constraint on the shape of clusters and better ability to account for structures of arbitrary shape (Rokach & Maimon, 2005; Han et al., 2011). We also tested the sensitivity of the clustering results (spatial patterns, annual cycle) to the number of PCs included (PC1 to PC5), there was a small influence of additional PCs on the results (reanalysis, models) over 1979-2017 and very small influence over 1979-2100 (increasing with the number of PCs; not shown). This reinforced our choice of using only PC1, considering that additional PCs represent little additional seasonality and difference in the long-term response of atmospheric circulation to climate change.

2.3 | Seasonal circulation regimes based on detrended data

The goal is now to remove the North Atlantic increase in Z500 to further investigate changes in Z500 patterns. This requires preserving both the spatial structures and the seasonality while removing the regional (North Atlantic) effect. Calculating and removing the trend by gridpoint would result in losing the spatial structures while doing so without a year of reference would result in losing the seasons. Therefore, the trend is calculated on the spatial mean of the whole area for each calendar day, with reference to 2017 (last year contained in both reanalyses and models). This means that for each specific day of the calendar year (1 Jan, 2 Jan, ..., 31 Dec), the trend is calculated with the 122 values (from 1979 to 2100) of the spatial mean for this specific day. The trend was estimated best by using a cubic smoothing spline (as in e.g. Jézéquel et al., 2020; Xu et al., 2021). Therefore, for each gridpoint and calendar day, we remove the spatial trend estimated by the spline from the raw Z500 (or TAS) values, and add the seasonal value of 2017 (also estimated by the spline)

to obtain the detrended data. The detrended SCRs (d-SCRs) are then obtained by applying the same method as before, of principal component analysis followed by clustering, to the detrended data. We heuristically chose to also detrend TAS (similarly to Z500) for the analysis of detrended data. We emphasize that the detrending removes the regional (North Atlantic) trend per calendar day so that the resulting local trend of the detrended data is the residual of the regional trend. A negative residual trend at a given gridpoint means that its Z500 values are increasing less than the regional average, or even are decreasing, whereas a positive residual trend means that the local trend is higher than that of the regional average.

3 | Results

The first part of the results focuses on the SCRs in ERAI and in the climate models over 1979-2017 to assess how the models perform with respect to the reanalyses. The second part examines SCRs in climate models over 1979-2100 to detect evolutions in the temporal and spatial structures. The third part explores the possible causes for the evolution of SCRs over 1979-2100, such as uniform (North Atlantic) Z500 increase, or changes in Z500 spatial patterns.

3.1 | Evaluation of past seasonal circulation regimes in climate models (1979-2017)

We start by looking at the spatial patterns of the regimes as shown by the composites maps in Figure 1. Each composite map is calculated by averaging the values of the Z500 fields corresponding to the days that belong to the regime, with color shading representing the seasonal anomalies and contour lines representing the raw values. The contours and fields are shown both in order to highlight the regime patterns in raw Z500 and the deviation of the regime patterns from the mean seasonal cycle of Z500. Seasonal anomalies correspond to the raw values minus the average seasonal cycle over 1979-2017. The average seasonal cycle is calculated by averaging the Z500 values per calendar day (1 Jan, ..., 31 Dec) over the 39 years. For climate models, each regime composite map is determined individually (i.e. average map) and the multimodel composite is calculated as the mean of the distribution of the twelve composites. The spatial patterns of the four average regimes found in the models are very similar to those from ERAI, and to those from Vrac et al. (2014) based on NCEP (National Center for Environmental Prediction) reanalyses. These patterns also share similarities and differences (detailed below) with the usual North-Atlantic weather regimes from the literature (e.g. Yiou & Nogaj (2004); Cassou (2008); Cattiaux et al. (2013); Hertig & Jacobeit (2014); Hannachi et al. (2017)).

The first regime (R1) corresponds to strong cyclonic conditions northward of 35°N and weakly anticyclonic southward (i.e. anomalously strong Westerly flow), and the

second regime (R2) to the opposite (weaker Westerly flow). R1 resembles the positive phase of the North Atlantic Oscillation (NAO+) and R2 its negative phase (NAO-; Hurrell et al. (2003)), but Z500 anomalies are weaker, more zonal and further South than in the usual Iceland-Azores dipole (North/South and East/West, as in e.g. Yiou & Nogaj (2004); Cassou (2008)). Therefore, our R1 and R2 represent dynamics that are different from the NAO and more akin to an annular mode. In addition, Scandinavia appears colder under R1 and warmer under R2, whereas it would be warmer under NAO+ and colder under NAO- (Cattiaux et al., 2013).

The third regime (R3) yields weak anticyclonic conditions over the Northwestern Atlantic and cyclonic from the Southwest towards the Northeast (biased in climate models), corresponding to a wavy jet stream, similarly to the Atlantic Ridge (AR) pattern but lacking the cyclonic conditions over Europe present in AR (Yiou & Nogaj, 2004; Cassou, 2008). The fourth regime (R4) yields strong anticyclonic conditions over Northwestern Europe, resembling the Scandinavian Blocking (SB) pattern except that SB is also associated to cyclonic conditions between Greenland and Northeastern America (Yiou & Nogaj, 2004; Cassou, 2008; Cattiaux et al., 2013).

The temporal patterns of our SCRs are based on full years (like Vrac et al. (2014)), unlike the literature considering weather patterns either in winter (e.g. Yiou & Nogaj (2004); Cassou (2008); Hertig & Jacobeit (2014); Fabiano et al. (2021)), or in summer (e.g. Folland et al. (2009); Guemas et al. (2010); Cattiaux et al. (2013)). Thus, if our SCRs share similarities with the usual weather regimes, they however present large differences in their definition and properties. Indeed, our regimes correspond rather to the variability of the seasonal cycle of atmospheric conditions, while the usual regimes correspond rather to the intra-seasonal variability of these conditions. The annual cycle of our regimes' monthly frequencies over 1979-2017 is shown in Figure 2. Climate models reproduce an annual cycle of SCRs similar to ERAI, with regime 1 (hereafter R1) representing a winter-like season, R4 a summer-like season, and R2 and R3 transitional seasons (R2 around winter and R3 around summer).

In general, the climate models reproduce atmospheric patterns (Z500, TAS) that are very similar to ERAI (Fig. 1 and Fig. 3), but individual models are less successful (see Table 2 and Figures S4-S11). For example, the circulation patterns associated with R1 and R3 in MIROC5 are very different from other climate models and ERAI (Figures S4 and S6), despite happening at the same period in the year (Fig. 2). All other climate models show R1 patterns similar to ERAI albeit with diverse intensities (Figure S4). Several climate models (e.g. BCC-CSM1-1M and MRI-ESM1) overestimate R1 seasonal anomalies of Z500 (negative in the North and positive in the South; cf. Figure S4), corresponding to a more positive North-to-South gradient (i.e. stronger Westerly flow) than observed in the reanalysis (also visible on Fig. 1) during December to March (Fig. 2). Models overestimating Westerly flow in R1 also tend to have larger surface temperature anomalies (Figure S8), more negative than observed (reanalysis) over North America, Greenland and Scandinavia, and more positive over parts of Europe.

In the case of R2 and R4, ERAI and all climate models agree on the circulation pattern but differ in intensity (Figures S5 and S7). The spatial patterns of R2 (Z500 and TAS) are almost symmetrical to those of R1 (Fig. 1 and 3), with several models overestimating positive anomalies in the North and negative anomalies in the South (Figure S5), corresponding to a more negative North-to-South gradient (i.e. weaker Westerly flow) than observed (also visible on Fig. 1) during March to May and October to December (Fig. 2). Models underestimating Westerly flow in R2 also tend to have larger surface temperature anomalies than observed (Figure S9), more positive over North America and Greenland, and more negative over parts of Europe. The biases of individual models (e.g. BCC-CSM1-1M and MRI-ESM1) in the spatial patterns of R2 (Z500 and TAS) are also symmetrical to R1 biases (Figures S4-S5 and S8-S9).

The representation of R3 in climate models appears inaccurate (location and intensity of pressure centers) by comparison to ERAI (Table 2 and Figure S6) in April to June and September to November (Fig. 2). Models also tend to have biased R3 TAS patterns (location and intensity; Figure S10), with for instance Greenland that is warmer in ERAI but colder in GFDL-CM3 and MIROC5. A few models (e.g. BCC-CSM1-1M and MRI-ESM1) overestimate the TAS anomalies over Greenland (positive) and Europe (negative).

For R4, several models underestimate anticyclonic conditions in the North or overestimate cyclonic conditions in the South (Figure S7), corresponding to weaker Westerly flow in June to September (Fig. 2). The overestimation of cyclonic conditions by models in R4 is associated to a cold bias (e.g. over Spain for BCC-CSM1-1M and MRI-ESM1; cf. Figure S11), while the overestimation of anticyclonic conditions is associated with a warm bias (e.g. over Northern Europe in BCC-CSM1-1M).

The variability between climate models, represented here by the standard deviation over the 12 values (one per regime composite of climate model), appears larger (Fig. 1) for winter regimes (R1 and R2 with large anomalies) than for summer regimes (R3 and R4 with weak anomalies). The same holds true for TAS spatial patterns associated to the regimes (Fig. 3).

After looking at the seasonal structure of the regimes, we then investigated if and how the temporal organisation of these regimes changed during 1979-2017 through (i) the regime monthly frequencies, (ii) the first (start) and last (end) days of regime occurrence, and (iii) the regime persistence (i.e. average number of consecutive days). Most changes in ERAI and in the average of the models were similar (not shown) to the results from Vrac et al. (2014): R1 (i.e. winter conditions) decreasing in frequency, starting slightly later, ending slightly earlier, and being less persistent, and the opposite for R4 (i.e., summer conditions).

3.2 | Future changes in seasonal circulation regimes (1979-2100)

We now use the same method as before to define SCRs but based on the full simulation datasets over 1979-2100 to detect potential future changes. The first approach is to use four regimes (SCR4). Between the first three decades (1979-2008) and the last three decades (2071-2100) of the period, R1 occurs less often but is more intense for both Z500 and TAS (Figures S12-S13). We emphasize here that the regimes are defined over 1979-2100 and that we investigate their main properties (spatial patterns, annual cycle) over the subperiods (1979-2008 and 2071-2100) by selecting the results of the full-period clustering over these subperiods. The seasonal anomalies are calculated with reference to the average seasonal cycle of the subperiod (1979-2008, 2071-2100). In the case of R4, it occurs more often with less intense patterns, i.e. becoming closer to the seasonal mean. R2 occurs more often but is less intense, while R3 occurs slightly less often but is more intense. Note that these patterns are relative to the seasonal mean, which increases substantially over the North Atlantic between the first and last three decades (averaging about +90 m for Z500 and +4°C for TAS; not shown).

A shift happens in the annual cycle of SCR4 over 1979-2100 with R1 shrinking, R2 and R3 moving towards the winter period of the year, and R4 growing (Figure S14). GFDL-CM3 stands out from the other GCMs (Global Circulation Models) by showing the emergence in the future of a new summer regime that almost did not exist in the past (one day of very wavy jet stream and large temperature anomalies, not shown). This emergence means that in the case of GFDL, the difference between historical and future Z500 conditions in summer is so large that a new regime was created in the clustering. As the clustering has little freedom with 4 clusters (i.e. large constraints on the definition of the regimes), this emergence is even more interesting, but it is consistent with stronger increase of Z500 and TAS in this climate model by comparison to other models (not shown). However, since future R4 in GFDL is very similar to future R4 from other models (annual cycle and spatial pattern, respectively shown in Figure S14 and not shown), and since R4 was already well established in the past for other models, this emergence of R4 in GFDL does not represent the emergence of a new regime from a general perspective.

Monthly frequencies show R2 taking the place of R1 in the December, January and February months (hereafter DJF) starting from the middle of the 21st century, and R4 taking the place of R3 in June around 2025 (not shown). Although the average between models shows a clear direction of SCR evolution, the timing of this evolution differs up to a few decades between individual models. In consistence with the seasonal shift of regimes, the average of climate models between 1979 and 2100 shows R1 starting about one month and a half later while ending about two months earlier, and persisting less, whereas R4 starts about one month earlier while ending about one month and a half later, and persists more (Figures S15-S16).

Over 1979-2100, the spatial patterns of SCR trends of Z500 and TAS are in agreement among GCMs (Figures S17- S18) and are more robust than over 1979-

2017. These maps of linear trends are obtained by calculating the linear regression of the evolution of the variable (raw values) by gridcell, grey areas correspond to trends that are not significant (p-value > 0.05). The unconditional trend corresponds to the linear fit over the whole period (all days), whereas
the regime-conditional trends are calculated by multiple linear regressions to account for the distribution of days between regimes (cf. Appendix). Both regression coefficients and p-values are calculated individually by climate model, and then averaged over the twelve values. However, these spatial patterns of SCR trends show different spatial evolutions between Z500 and TAS within regimes, hence partially decoupled evolutions of atmospheric dynamics and surface temperature.
Even if using four regimes allows us to explore the future with a traditional number of seasons, the low number of clusters limits the freedom of the clustering to allow the appearance or disappearance of significant structures. Therefore, we applied a second approach to overcome this limit. We tested different numbers of regimes (up to 10) and chose seven regimes as a showcase because it corresponds to an optimization of the BIC (Figure S19) and illustrates the clearest transitions between the disappearance of past structures and appearance of future (new) structures.
With seven regimes (SCR7), the patterns of atmospheric circulation are very similar to those of surface temperatures (i.e. cyclonic associated to cold, anticyclonic to warm) in both past (1979-2008) and future (2071-2100) (Fig. 4-5). Regime patterns seem to follow the seasonal cycle (pale colors) except for R1, R2 and R7. Past (1979-2008) R7 cor responds to rare and very intense anticyclonic conditions over the Northern half of the region in association with summer heatwaves over the continents of the North Atlantic region (except North Africa and northernmost Canada).
Future (2071-2100) R1 corresponds to rare and very intense NAO+ conditions associated with cold spells over North eastern America, Greenland and Scandinavia. Here, we use the terms "cold spell" and "heatwave" to designate robust anomalies (average of more than 50 days i.e. 50 values) over large areas (continents) of about 3°C relative to the average seasonal cycle.
Overall, we observe a shift in the spatial patterns (Z500 and TAS) of the regimes (Fig. 4-5) with past R1 patterns becoming future R2 patterns, past R2 patterns becoming future R3 patterns, and so on until R6, while the R1 pattern becomes seasonally more extreme (rarer and more intense pattern) and the R7 pattern becomes seasonally more normal (more frequent and less intense pattern). We calculated the average monthly frequency of the seven regimes in a similar way to Fig. 2 but over the first three decades (1979-2008) and the last three decades (2071-2100), shown in Figure 6. R7 is a new summer regime almost absent in the past period (1979-2008) that replaces R6 and “pushes” all the other regimes towards the winter calendar days while R1 (past or old winter regime) disappears. This shift in the annual cycle of the regimes between past and future appears very consistent with the shift in the regime spatial patterns.
The timing of these changes in regime occurrence during the year can be investigated through the monthly frequencies of the regimes over 1979-2100 (winter

months in Fig. 7 and summer months in Fig. 8). Figure 7 shows the collapse of R1 happening throughout the 21st century. R2 takes the place of R1 in the beginning of the 21st century, and becomes replaced by R3 at the end of the 21st century. Symmetrically, R6 is replaced by R7 during the second half of the 21st century (Fig. 8). The evolution of the starting and ending dates as well as persistence of all regimes are consistent with the evolution of their annual cycle and monthly occurrence (Figures S20-S21). Summertime regimes (R5 to R7 in June to September; Fig. 6) start earlier and end later over 1979-2100, while other regimes start later and end earlier (Figure S20). The average persistence of R1 and R6 decreases over 1979-2100, while that of intermediary regimes remains about 5-10 days, and that of R7 increases dramatically (Figure S21).
All regimes except R7 show a similar pattern of Z500 change over the region: increase in the Southern part and decrease in the Northern part, whereas R7 shows widespread increase that is stronger in the South and not robust among climate models in the North of the region (Figure S22). Interestingly, these changes in circulation patterns seem to be opposite to the expected effects from Arctic amplification, such as amplified warming and geopotential height increase over circulation dynamics that are linked to midlatitude weather (Cohen et al., 2014; Barnes & Polvani, 2015; Overland et al., 2015). The strongest warming over the region is observed in R1 and R7, whereas R3 to R6 show (unexpected) cooling over the continents (Figure S23). The origin of this cooling is investigated later in the discussion of the paper (Section 4.3). The appearance and disappearance of regimes observed in SCR7 over 1979-2100 is absent from the 1979-2017 period where we tested with four up to seven regimes.

3.3 | Seasonal circulation regimes based on detrended data (1979-2100)

The increasing trend of Z500 over the North Atlantic region, mainly due to human influence (Christidis & Stott, 2015), is expected to be driving the evolution of the SCRs but changes in spatial patterns could also play a role. To investigate this, we use SCRs based on detrended data (d-SCRs) and focus on the average d-SCRs of climate models. This detrending corresponds to removing the trend of the regional average Z500 (or TAS, see Methods 2.3) for each calendar day individually. By comparison to SCRs, the temporal structures of d-SCRs over 1979-2100 appear almost stationary and remain very similar to those of ERAI (Fig. 9). However, spatial structures of d-SCRs present some minor variability for Z500 (Fig. 10) but major changes for TAS in which case future patterns are almost symmetrically opposite to past patterns (Fig. 11). This small evolution of Z500 spatial patterns in d-SCRs can be explained by trends that are either not significant in individual climate models or in disagreement between climate models, as shown by large greyed areas in Figure S24. However, most of the TAS trends in d-SCRs are robust and show warming over continents and reduced warming over oceans (Figure S25). This warming contrast

can be explained because of the higher heat capacity and evaporative cooling potential of ocean surface than land surface, and ocean mixing (Dai, 2016). These trends also show Arctic amplification (i.e. warming stronger at the pole than at lower latitudes), especially in winter (R1 to R3).

The next analysis aims to determine the causes of the changes in Z500 and TAS patterns within SCRs and d-SCRs. The North Atlantic increase in Z500 and TAS (hereafter NAI) and the seasonal shift of regimes (hereafter SS) could both play a role in these changes. Figures S26-S27 show the effect of NAI (without SS), through regime composite maps calculated on raw Z500 (or raw TAS) but conditionally to the clusters defined on detrended Z500 (i.e. clusters with almost constant temporal structures). The contribution of NAI corresponds only to widespread increasing Z500 and TAS in all regimes. Figures S28-S29 show the effect of SS (without NAI), through the regime composite maps calculated on detrended Z500 (or detrended TAS) but conditionally to the clusters defined on raw Z500. The shift of SCRs towards winter corresponds to widespread decreasing Z500 and TAS in most regimes (except R1, R2, and unconditionally to regimes). Therefore, the two opposing effects of NAI and SS can explain the existence of decreasing trends of Z500 and TAS observed earlier within SCRs.

4 | CONCLUSIVE DISCUSSIONS

We used seasonal circulation patterns (Vrac et al., 2014) by clustering Z500 from the ERAI reanalysis and 12 CMIP5 climate models to study past (1979-2017) and future (1979-2100) seasonal structures of mid-troposphere atmospheric dynamics (Z500) and air surface temperature (TAS) over the North Atlantic region and their evolutions in time.

4.1 | Ability of climate models to represent past seasonal variability

The comparison of climate models with ERAI over 1979-2017 showed small biases in the four seasonal circulation regimes (spatial pattern, time of occurrence). On average, the circulation regimes from the climate models are very similar to those from ERAI. However, we identified larger biases in individual climate models. For instance, several models (e.g. in BCC-CSM1-1M and MRI-ESM1) overestimate the meridional gradients in R1, corresponding to an overestimation of wintertime (December-March) westerly flow. This wintertime tendency of models to overestimate Westerly flow leads to the overestimation of surface temperatures (as in Wójcik (2015)). Similarly, the underestimation of Westerly flow in R2 by several models (during March-May and October-December) leads to overestimated temperature anomalies. These biases in atmospheric flow and surface temperatures are commonly linked to the overestimation of the wintertime jetstream (strength and

stability) in GCMs due to their coarse horizontal resolution (Scaife et al., 2010; Dawson et al., 2012; Iqbal et al., 2018).
R3 is the most biased atmospheric regime in climate models, with several models simulating inaccurate patterns (location, intensity) of Z500 and TAS in April-June and September-November. These biases are likely due to the tendency from models of simulating a jetstream (or storm track) that is too zonal and underestimating its frequency of meandering (Scaife et al., 2010; Cattiaux et al., 2013; Zappa et al., 2013; Iqbal et al., 2018), in consistence with stronger Z500 meridional gradient and faster zonal wind in models than observed (Hassanzadeh et al., 2014; Wójcik, 2015; Cattiaux et al., 2016). In the case of R4, the overestimation of cyclonic conditions (cold bias) and underestimation of anticyclonic conditions (warm bias) by several models can be linked to a model tendency of underestimating summertime (June-September) Westerly flow and jetstream windspeed (Iqbal et al., 2018).
Despite biases in the climate model representation of Z500 and TAS seasonal variability, the general evolution of the four seasonal circulation regimes (SCR4) over 1979-2017 was consistent between models and ERAI: decreasing frequencies of historical winter conditions and increasing frequencies of historical summer conditions of atmospheric dynamics. Most of the results agree with the findings of Vrac et al. (2014), except that we detect a more pronounced winter evolution. This is probably because their reanalysis dataset covered 1948-2011 while our data covers 1979-2017, which is more recent and better captures global warming (section 2.4.1.1 and Table 2.4 in IPCC (2013)). The structures (spatial, temporal) and evolution (timing) of SCRs differ between climate models over 1979-2017 and even more over 1979-2100.

4.2 | Projected evolutions of seasons

When looking at future (1979-2100) evolutions of SCRs with both four and seven regimes, the frequency of historical winter conditions decreases while that of historical summer conditions increases and occurrences of transitional regimes move towards the winter period. These changes are attached to large increases in the seasonal mean of Z500 and TAS over the North Atlantic. The results for summer (lengthening) are consistent with those of Cassou & Cattiaux (2016) but not the results for winter (shortening), which could be due to the very different methods used to define seasonality. Moreover, allowing for more freedom in the definition of the SCRs by using seven regimes rather than four, we find a collapse of the regime associated to past winter conditions, corresponding to rare cold spells at the end of the 21st century, and the growth of a new summer regime corresponding to past heatwaves that becomes dominant in summer by the end of the 21st century.
These results suggest that past winter conditions are becoming shorter in time and past summer conditions are broadening and intensifying, in consistence with changing thermal seasons (Peña-Ortiz et al., 2015; Ruosteenoja et al., 2020; Wang et al., 2021). However, in our case the apparent changes in seasonality seem to correspond rather to a swap between regimes since occurrences of past R1 are

replaced by R2 in the future, past R2 are replaced by R3, and so on until R6. Note that R1 conditions correspond to the past winter pattern that almost disappears at the end of the 21st century. Hence, for the future projections, R1 corresponds to extreme winter (rare intense Westerly flow) with respect to the “normal” future seasonality. Therefore, this regime swap, with symmetry between spatial patterns and annual cycle, suggests that the seasonality of the atmospheric patterns does not change in a major way relative to the evolution of the raw seasonal cycle of Z500 and TAS.

Over the last three decades (2071-2100) respectively to the first three decades (1979-2008), SCR4 had about 75% fewer days (on average between climate models) of enhanced Westerly flow (R1) and about 10% of wavy jetstream (R3) but about 54% more days of weakened Westerly flow (R2) and 135% more days of anticyclonic conditions (R4). Under future warming, this increasing frequency of weakened Westerly flow in winter and anticyclonic conditions over Europe in summer is consistent with the findings from Cattiaux et al. (2013), associated to a reduction of snow cover in winter and of cloudiness in summer. The increase in the frequency of anticyclonic conditions during May, June, September and October could have consequences for extreme events, such as heatwaves and dry spells as Röthlisberger & Martius (2019) found a strong positive effect of atmospheric blocking conditions on the persistence of simultaneously occurring hot and dry spells over Europe between May and October.

Additionally, the findings from Pfleiderer et al. (2019) that summer weather becomes more persistent in a warmer world, although they consider summer in June-July-August, can be linked to our finding of an increase in summer regime persistence. SCR4 over 1979-2100 also revealed a weakening in the patterns of weakened Westerly flow and anticyclonic conditions (R2 and R4), and a strengthening in the patterns of enhanced Westerly flow and wavy jetstream (R1 and R3) at the end of the 21st century by comparison to the end of the 20th century. This future strengthening of the enhanced Westerly flow (R1) pattern in the winter period is consistent with a decrease of cold spells over Europe (Peings et al., 2013) as they are facilitated by anticyclonic conditions in winter (Buehler et al., 2011). The strengthening of the wavy jetstream (R3) pattern and weakening of anticyclonic (R4) pattern can be put in relation with the suggestion from Christidis & Stott (2015) that the relative Z500 increase between polar and mid-latitude regions in the Northern Hemisphere could moderate the westerly flow over the North Atlantic and affect the positioning of the North Atlantic jet stream, especially with a change in the sinuosity of the midlatitude atmospheric flow (Cattiaux et al., 2016).

4.3 | Drivers of the evolution(s)

The appearance and disappearance of regimes over 1979-2100 do not happen in 1979-2017, probably due to the smaller scale of change in Z500 in this period by contrast to the future where the full extent of the emission scenarios kick in inside the climate model simulations. We found that the trends of increasing and decreasing

Z500 within regimes, generally associated respectively to TAS warming and cooling trends, are the result of two opposite processes: the North Atlantic increase in Z500 due to human influence, and the seasonal shift of regimes towards the winter period, where Z500 and TAS are lower than during the rest of the year. This seasonal shift explains the decreasing Z500 trends, generally associated with cooling, which are observed in several regions within SCRs and would otherwise not be possible. This explanation also covers the cooling trends reported by Vrac et al. (2014), understood here as a temporal shift of the regimes' occurrences towards the winter period with cooler conditions rather than a seasonally-stationary cooling.
The d-SCRs results (i.e. SCRs obtained from detrended Z500) showed almost no temporal evolution between past and future, which means that the North Atlantic increase in Z500 is the main cause for the evolution of SCRs. Christidis & Stott (2015) reported that the planetary Z500 increase during 1979-2012 was mostly due to human forcings. So, although climate models overestimate the surface warming and Z500 increase over the past period (Jones et al., 2013; Christidis & Stott, 2015), human forcings appear to cause the shift in seasonality of the regimes that we detect here, since most of the evolution of the regimes disappears when we remove the North Atlantic increase in Z500.

4.4 | Limitations and perspectives

Even though the regimes and their evolutions in climate models in the past period are similar to those from ERAI, we note a few limitations and sources of uncertainty. The representation of the climate in ERAI and models has uncertainties and errors, especially in atmospheric dynamics (Shepherd, 2014) and surface temperature in models (Jones et al., 2013). Bias correction methods could lead to more realistic seasonal atmospheric regimes but could imply other issues such as modifications of spatial and temporal structures (and trends) that could possibly generate physical inconsistencies (Vrac, 2018; François et al., 2020).
Overall, although our study highlights the value of a clustering approach for comparing (and evaluating) models as well as seasonal structures, the apparent consistency that we find between climate models on the future evolution of seasonal dynamics seems at odds with other studies where the projected circulation response differs strongly between models (e.g. Barnes & Polvani (2015)). Indeed, clustering approaches might hide inter-model variability, or seasonal variability (depending on the number of clusters). Additional sources of uncertainty include the choice of RCP8.5 for the future emission scenarios and the choice of Z500 (i.e., mid-troposphere atmospheric circulation) rather than surface, lower or higher troposphere.
Three outlooks emerge from this study. First, the model dependency on the changes in atmospheric circulation could be examined further, by comparing the model regime biases to the mean model biases in atmospheric flow climatology. Second, the link between regional warming and circulation changes could also be investigated further, by comparing regime changes to model climate sensitivity. In

other words, does more warming correspond to earlier and stronger changes in circulation seasonality during the century? Third, the local-scale implications of the large-scale circulation changes could be clarified further, by downscaling meteorological variables (e.g. temperature, precipitation, windspeed) based on the large-scale circulation regimes (Vrac & Yiou, 2010). Another way to characterize the local climate shifts would be to use climate analogs, to identify future impacts, vulnerabilities, and adaptation options (Rohat et al., 2018; Bastin et al., 2019). Understanding the effect of climate change on seasonality is important to anticipate future changes in weather conditions and the consequences for nature and society.

Supporting information

Figures S1 to S29 can be found in the Supporting Information associated to this article.

Code and data availability

The ERAI data is available at https://www.ecmwf.int/en/forecasts/datasets/reanalysis-datasets/era-interim. The CMIP5 data is available at https://esgf-node.ipsl.upmc.fr/search/cmip5-ipsl/. The computations were done using the free statistical package mclust (Scrucca & Raftery, 2015) on the R software (www.r-project.org).

Acknowledgements

The authors thank Soulivanh Thao, Ara Arakelian, and Flavio Pons for technical assistance. We also thank Christophe Cassou for suggestions of perspectives, and the reviewers from the International Journal of Climatology for their recommendations that helped to improve the article. FB and MV acknowledge financial support from the CoCliServ project. MV and PY also acknowledge support from the EUPHEME project. Both CoCliServ and EUPHEME are part of ERA4CS, an ERA-NET initiated by JPI Climate and co-funded by the European Union.

Conflict of interest

The authors do not have competing interests to declare.

References

Adachi, Y., Yukimoto, S., Deushi, M., Obata, A., Nakano, H., Tanaka, T. Y., ... & Kitoh, A. (2013). Basic performance of a new earth system model of the Meteorological Research Institute (MRI-ESM1). *Pap. Meteorol. Geophys*, *64*, 1-19.

Angell, J. K., & Korshover, T. (1974). Quasi-biennial and long-term fluctuations in the centers of action. Monthly Weather Review, 102(10), 669-678.

Barnes, E. A., & Polvani, L. M. (2015). CMIP5 projections of Arctic amplification, of the North American/North Atlantic circulation, and of their relationship. Journal of Climate, 28(13), 5254-5271.

Barnston, A. G., & Livezey, R. E. (1987). Classification, seasonality and persistence of low-frequency atmospheric circulation patterns. *Monthly weather review*, *115*(6), 1083-1126.

Bentsen, M., Bethke, I., Debernard, J. B., Iversen, T., Kirkevåg, A., Seland, Ø., ... & Kristjansson, J. E. (2013). The Norwegian Earth System Model, NorESM1-M–Part 1: description and basic evaluation of the physical climate. *Geoscientific Model Development*, *6*(3), 687-720.

Hoegh-Guldberg, O., Jacob, D., Bindi, M., Brown, S., Camilloni, I., Diedhiou, A., ... & Zougmoré, R. B. (2018). Impacts of 1.5 C global warming on natural and human systems. *Global warming of 1.5 C. An IPCC Special Report*.

Blackmon, M. L., Lee, Y. H., & Wallace, J. M. (1984). Horizontal structure of 500 mb height fluctuations with long, intermediate and short time scales. *Journal of Atmospheric Sciences*, *41*(6), 961-980.

Brunner, L., Schaller, N., Anstey, J., Sillmann, J., & Steiner, A. K. (2018). Dependence of present and future European temperature extremes on the location of atmospheric blocking. *Geophysical research letters*, *45*(12), 6311-6320.

Buehler, T., Raible, C. C., & Stocker, T. F. (2011). The relationship of winter season North Atlantic blocking frequencies to extreme cold or dry spells in the ERA-40. *Tellus A: Dynamic Meteorology and Oceanography*, *63*(2), 174-187.

Cassou, C. (2008). Intraseasonal interaction between the Madden–Julian oscillation and the North Atlantic Oscillation. *Nature*, *455*(7212), 523-527.

Cassou, C., & Cattiaux, J. (2016). Disruption of the European climate seasonal clock in a warming world. *Nature Climate Change*, *6*(6), 589-594.

Cattiaux, J. (2010). *Extrêmes de température en Europe: mécanismes et réponses au changement climatique* (Doctoral dissertation, Paris 6).

Cattiaux, J., Douville, H., & Peings, Y. (2013). European temperatures in CMIP5: origins of present-day biases and future uncertainties. *Climate dynamics*, *41*(11-12), 2889-2907.

Cattiaux, J., Peings, Y., Saint-Martin, D., Trou-Kechout, N., & Vavrus, S. J. (2016). Sinuosity of midlatitude atmospheric flow in a warming world. *Geophysical Research Letters*, *43*(15), 8259-8268.

Cattiaux, J., Yiou, P., & Vautard, R. (2012). Dynamics of future seasonal temperature trends and extremes in Europe: a multi-model analysis from CMIP3. *Climate dynamics*, *38*(9-10), 1949-1964.

Christidis, N., & Stott, P. A. (2015). Changes in the geopotential height at 500 hPa under the influence of external climatic forcings. *Geophysical Research Letters*, *42*(24), 10-798.

Chylek, P., Li, J., Dubey, M. K., Wang, M., & Lesins, G. J. A. C. (2011). Observed and model simulated 20th century Arctic temperature variability: Canadian earth system model CanESM2. *Atmospheric Chemistry and Physics Discussions*, *11*(8), 22893-22907.

Cohen, J., Screen, J. A., Furtado, J. C., Barlow, M., Whittleston, D., Coumou, D., ... & Jones, J. (2014). Recent Arctic amplification and extreme mid-latitude weather. *Nature geoscience*, *7*(9), 627-637.

Collier, M., & Uhe, P. (2012). *CMIP5 datasets from the ACCESS1.0 and ACCESS1.3 coupled climate models*. Centre for Australian weather and Climate Research.

Dai, A. (2016). Future warming patterns linked to today's climate variability. *Scientific reports*, *6*(1), 1-6.

Dawson, A., Palmer, T. N., & Corti, S. (2012). Simulating regime structures in weather and climate prediction models. *Geophysical Research Letters*, *39*(21).

Dee, D. P., Uppala, S. M., Simmons, A. J., Berrisford, P., Poli, P., Kobayashi, S., ... & Vitart, F. (2011). The ERA-Interim reanalysis: Configuration and performance of the data assimilation system. *Quarterly Journal of the royal meteorological society*, *137*(656), 553-597.

Dempster, A. P., Laird, N. M., & Rubin, D. B. (1977). Maximum likelihood from incomplete data via the EM algorithm. *Journal of the Royal Statistical Society: Series B (Methodological)*, *39*(1), 1-22.

Díaz-Esteban, Y., Raga, G. B., & Díaz Rodríguez, O. O. (2020). A weather-pattern-based evaluation of the performance of CMIP5 models over Mexico. *Climate*, *8*(1), 5.

Dufresne, J. L., Foujols, M. A., Denvil, S., Caubel, A., Marti, O., Aumont, O., ... & Vuichard, N. (2013). Climate change projections using the IPSL-CM5 Earth System Model: from CMIP3 to CMIP5. *Climate dynamics*, *40*(9), 2123-2165.

Estivill-Castro, V., & Yang, J. (2000, August). Fast and robust general purpose clustering algorithms. In *Pacific Rim International Conference on Artificial Intelligence* (pp. 208-218). Springer, Berlin, Heidelberg.

Fabiano, F., Christensen, H. M., Strommen, K., Athanasiadis, P., Baker, A., Schiemann, R., & Corti, S. (2020). Euro-Atlantic weather Regimes in the PRIMAVERA coupled climate simulations: impact of resolution and mean state biases on model performance. *Climate Dynamics*, *54*, 5031-5048.

Fabiano, F., Meccia, V. L., Davini, P., Ghinassi, P., & Corti, S. (2021). A regime view of future atmospheric circulation changes in northern mid-latitudes. *Weather and Climate Dynamics*, *2*(1), 163-180.

Folland, C. K., Knight, J., Linderholm, H. W., Fereday, D., Ineson, S., & Hurrell, J. W. (2009). The summer North Atlantic Oscillation: past, present, and future. *Journal of Climate*, *22*(5), 1082-1103.

Fraley, C., & Raftery, A. E. (2002). Model-based clustering, discriminant analysis, and density estimation. *Journal of the American statistical Association*, *97*(458), 611-631.

Franzke, C., Woollings, T., & Martius, O. (2011). Persistent circulation regimes and preferred regime transitions in the North Atlantic. *Journal of the atmospheric sciences*, *68*(12), 2809-2825.

François, B., Vrac, M., Cannon, A. J., Robin, Y., & Allard, D. (2020). Multivariate bias corrections of climate simulations: which benefits for which losses?. *Earth System Dynamics*, *11*(2), 537-562.

Giorgetta, M. A., Jungclaus, J., Reick, C. H., Legutke, S., Bader, J., Böttinger, M., ... & Stevens, B. (2013). Climate and carbon cycle changes from 1850 to 2100 in MPI-ESM simulations for the Coupled Model Intercomparison Project phase 5. *Journal of Advances in Modeling Earth Systems*, *5*(3), 572-597.

Griffies, S. M., Winton, M., Donner, L. J., Horowitz, L. W., Downes, S. M., Farneti, R., ... & Zadeh, N. (2011). The GFDL CM3 coupled climate model: characteristics of the ocean and sea ice simulations. *Journal of Climate*, *24*(13), 3520-3544.

Guemas, V., Salas-Mélia, D., Kageyama, M., Giordani, H., Voldoire, A., & Sanchez-Gomez, E. (2010). Summer interactions between weather regimes and surface ocean in the North-Atlantic region. *Climate dynamics*, *34*(4), 527-546.

Hannachi, A., Straus, D. M., Franzke, C. L., Corti, S., & Woollings, T. (2017). Low-frequency nonlinearity and regime behavior in the Northern Hemisphere extratropical atmosphere. *Reviews of Geophysics*, *55*(1), 199-234.

Hassanzadeh, P., Kuang, Z., & Farrell, B. F. (2014). Responses of midlatitude blocks and wave amplitude to changes in the meridional temperature gradient in an idealized dry GCM. *Geophysical Research Letters*, *41*(14), 5223-5232.

Hertig, E., & Jacobeit, J. (2014). Variability of weather regimes in the North Atlantic-European area: past and future. *Atmospheric Science Letters*, *15*(4), 314-320.

Hurrell, J. W., & Deser, C. (2010). North Atlantic climate variability: the role of the North Atlantic Oscillation. *Journal of marine systems*, *79*(3-4), 231-244.

Hurrell, J. W., Kushnir, Y., Ottersen, G., & Visbeck, M. (2003). An overview of the North Atlantic oscillation. *Geophysical Monograph-American Geophysical Union*, *134*, 1-36.

IPCC (2013). Climate Change 2013: The Physical Science Basis. Contribution of Working Group I to the Fifth Assessment Report of the Intergovernmental Panel on Climate Change [Stocker, T.F., D. Qin, G.-K. Plattner, M. Tignor, S.K. Allen, J. Boschung, A. Nauels, Y. Xia, V. Bex and P.M. Midgley (eds.)]. Cambridge University Press, Cambridge, United Kingdom and New York, NY, USA, 1535 pp.

Iqbal, W., Leung, W. N., & Hannachi, A. (2018). Analysis of the variability of the North Atlantic eddy-driven jet stream in CMIP5. *Climate Dynamics*, *51*(1), 235-247.

Jézéquel, A., Bevacqua, E., d'Andrea, F., Thao, S., Vautard, R., Vrac, M., & Yiou, P. (2020). Conditional and residual trends of singular hot days in Europe. *Environmental Research Letters*, *15*(6), 064018.

Jia, G. Coauthors, 2019: Land–climate interactions. *Climate Change and Land: An IPCC Special Report on Climate Change, Desertification, Land Degradation, Sustainable Land Management, Food Security, and Greenhouse Gas Fluxes in Terrestrial Ecosystems, J. Skea et al., Eds., IPCC*, 131-247.

Jones, C., Hughes, J. K., Bellouin, N., Hardiman, S. C., Jones, G. S., Knight, J., ... & Zerroukat, M. (2011). The HadGEM2-ES implementation of CMIP5 centennial simulations. *Geoscientific Model Development*, *4*(3), 543-570.

Jones, G. S., Stott, P. A., & Christidis, N. (2013). Attribution of observed historical near–surface temperature variations to anthropogenic and natural causes using CMIP5 simulations. *Journal of Geophysical Research: Atmospheres*, *118*(10), 4001-4024.

Lamb, H. H. (1950). Types and spells of weather around the year in the British Isles: Annual trends, seasonal structure of the year, singularities. *Quarterly Journal of the Royal Meteorological Society*, *76*(330), 393-429.

Lhotka, O., & Kyselý, J. (2015). Characterizing joint effects of spatial extent, temperature magnitude and duration of heat waves and cold spells over Central Europe. *International Journal of Climatology*, *35*(7), 1232-1244.

Rokach, L., & Maimon, O. (2005). Clustering methods. In *Data mining and knowledge discovery handbook* (pp. 321-352). Springer, Boston, MA.

Marshall, J., Kushnir, Y., Battisti, D., Chang, P., Czaja, A., Dickson, R., ... & Visbeck, M. (2001). North Atlantic climate variability: phenomena, impacts and mechanisms. *International Journal of Climatology: A Journal of the Royal Meteorological Society*, *21*(15), 1863-1898.

Overland, J., Francis, J. A., Hall, R., Hanna, E., Kim, S. J., & Vihma, T. (2015). The melting Arctic and midlatitude weather patterns: Are they connected?. *Journal of Climate*, *28*(20), 7917-7932.

Pearson, K. (1894). Contributions to the mathematical theory of evolution. *Philosophical Transactions of the Royal Society of London. A*, *185*, 71-110.

Peel, D., & McLachlan, G. J. (2000). Robust mixture modelling using the t distribution. *Statistics and computing*, *10*(4), 339-348.

Peings, Y., Cattiaux, J., & Douville, H. (2013). Evaluation and response of winter cold spells over Western Europe in CMIP5 models. *Climate dynamics*, *41*(11-12), 3025-3037.

Peña-Ortiz, C., Barriopedro, D., & García-Herrera, R. (2015). Multidecadal variability of the summer length in Europe. *Journal of Climate*, *28*(13), 5375-5388.

Pfleiderer, P., Schleussner, C. F., Kornhuber, K., & Coumou, D. (2019). Summer weather becomes more persistent in a 2°C world. *Nature Climate Change*, *9*(9), 666-671.

Philipp, A., Bartholy, J., Beck, C., Erpicum, M., Esteban, P., Fettweis, X., ... & Tymvios, F. S. (2010). Cost733cat–A database of weather and circulation type classifications. *Physics and Chemistry of the Earth, Parts A/B/C*, *35*(9-12), 360-373.

Price, J. M., & Magaard, L. (1986). Interannual baroclinic Rossby waves in the midlatitude North Atlantic. *Journal of physical oceanography*, *16*(12), 2061-2070.

Reinhold, B. B., & Pierrehumbert, R. T. (1982). Dynamics of weather regimes: Quasi-stationary waves and blocking. *Monthly Weather Review*, *110*(9), 1105-1145.

Rex, D. F. (1950). Blocking action in the middle troposphere and its effect upon regional climate. *Tellus*, *2*(4), 275-301.

Röthlisberger, M., & Martius, O. (2019). Quantifying the local effect of Northern Hemisphere atmospheric blocks on the persistence of summer hot and dry spells. *Geophysical Research Letters*, *46*(16), 10101-10111.

Ruosteenoja, K., Markkanen, T., & Räisänen, J. (2020). Thermal seasons in northern Europe in projected future climate. *International Journal of Climatology*, *40*(10), 4444-4462.

Sanchez-Gomez, E., Somot, S., & Déqué, M. (2009). Ability of an ensemble of regional climate models to reproduce weather regimes over Europe-Atlantic during the period 1961–2000. *Climate Dynamics*, *33*(5), 723-736.

Scaife, A. A., Woollings, T., Knight, J., Martin, G., & Hinton, T. (2010). Atmospheric blocking and mean biases in climate models. *Journal of Climate*, *23*(23), 6143-6152.

Schaller, N., Sillmann, J., Anstey, J., Fischer, E. M., Grams, C. M., & Russo, S. (2018). Influence of blocking on Northern European and Western Russian heatwaves in large climate model ensembles. *Environmental Research Letters*, *13*(5), 054015.

Schwalm, C. R., Glendon, S., & Duffy, P. B. (2020a). RCP8. 5 tracks cumulative CO2 emissions. *Proceedings of the National Academy of Sciences*, *117*(33), 19656-19657.

Schwalm, C. R., Glendon, S., & Duffy, P. B. (2020b). Reply to Hausfather and Peters: RCP8. 5 is neither problematic nor misleading. *Proceedings of the National Academy of Sciences*, *117*(45), 27793-27794.

Schwarz, G. (1978). Estimating the dimension of a model. *The annals of statistics*, 461-464.

Scrucca, L., & Raftery, A. E. (2015). Improved initialisation of model-based clustering using Gaussian hierarchical partitions. *Advances in data analysis and classification*, *9*(4), 447-460.

Shepherd, T. G. (2014). Atmospheric circulation as a source of uncertainty in climate change projections. *Nature Geoscience*, *7*(10), 703-708.

Sillmann, J., Croci-Maspoli, M., Kallache, M., & Katz, R. W. (2011). Extreme cold winter temperatures in Europe under the influence of North Atlantic atmospheric blocking. *Journal of Climate*, *24*(22), 5899-5913.

Stendel, M., Francis, J., White, R., Williams, P. D., & Woollings, T. (2021). The jet stream and climate change. In *Climate Change* (pp. 327-357). Elsevier.

Taylor, K. E., Stouffer, R. J., & Meehl, G. A. (2012). An overview of CMIP5 and the experiment design. *Bulletin of the American Meteorological Society*, *93*(4), 485-498.

Vautard, R. (1990). Multiple weather regimes over the North Atlantic: Analysis of precursors and successors. *Monthly weather review*, *118*(10), 2056-2081.

Voldoire, A., Sanchez-Gomez, E., y Mélia, D. S., Decharme, B., Cassou, C., Sénési, S., ... & Chauvin, F. (2013). The CNRM-CM5. 1 global climate model: description and basic evaluation. *Climate dynamics*, *40*(9), 2091-2121.

Vrac, M. (2018). Multivariate bias adjustment of high-dimensional climate simulations: the Rank Resampling for Distributions and Dependences (R2D2) bias correction. *Hydrology and Earth System Sciences*, *22*(6), 3175-3196.

Vrac, M., Hayhoe, K., & Stein, M. (2007). Identification and intermodel comparison of seasonal circulation patterns over North America. *International Journal of Climatology: A Journal of the Royal Meteorological Society*, *27*(5), 603-620.

Vrac, M., Vaittinada Ayar, P., & Yiou, P. (2014). Trends and variability of seasonal weather regimes. *International journal of climatology*, *34*(2), 472-480.

Vrac, M., & Yiou, P. (2010). Weather regimes designed for local precipitation modeling: Application to the Mediterranean basin. *Journal of Geophysical Research: Atmospheres*, *115*(D12).

Wallace, J. M., Zhang, Y., & Lau, K. H. (1993). Structure and seasonality of interannual and interdecadal variability of the geopotential height and temperature fields in the Northern Hemisphere troposphere. *Journal of Climate*, *6*(11), 2063-2082.

Wang, C. (2002). Atlantic climate variability and its associated atmospheric circulation cells. *Journal of climate*, *15*(13), 1516-1536.

Wang, J., Guan, Y., Wu, L., Guan, X., Cai, W., Huang, J., ... & Zhang, B. (2021). Changing lengths of the Four Seasons by global warming. *Geophysical Research Letters*, *48*(6), e2020GL091753.

Watanabe, M., Suzuki, T., O'ishi, R., Komuro, Y., Watanabe, S., Emori, S., ... & Kimoto, M. (2010). Improved climate simulation by MIROC5: Mean states, variability, and climate sensitivity. *Journal of Climate*, *23*(23), 6312-6335.

Wójcik, R. (2015). Reliability of CMIP5 GCM simulations in reproducing atmospheric circulation over Europe and the North Atlantic: a statistical downscaling perspective. *International Journal of Climatology*, *35*(5), 714-732.

Woollings, T., Hannachi, A., & Hoskins, B. (2010). Variability of the North Atlantic eddy-driven jet stream. *Quarterly Journal of the Royal Meteorological Society*, *136*(649), 856-868.

Wu, T., Song, L., Li, W., Wang, Z., Zhang, H., Xin, X., ... & Zhou, M. (2014). An overview of BCC climate system model development and application for climate change studies. *Journal of Meteorological Research*, *28*(1), 34-56.

Xu, P., Wang, L., Huang, P., & Chen, W. (2021). Disentangling dynamical and thermodynamical contributions to the record-breaking heatwave over Central Europe in June 2019. *Atmospheric Research*, *252*, 105446.

Yiou, P., & Nogaj, M. (2004). Extreme climatic events and weather regimes over the North Atlantic: when and where?. *Geophysical Research Letters*, *31*(7). https://doi.org/10.1029/2003GL019119

Zappa, G., Shaffrey, L. C., & Hodges, K. I. (2013). The ability of CMIP5 models to simulate North Atlantic extratropical cyclones. *Journal of Climate*, *26*(15), 5379-5396.

Tables

Table 1. Characteristics of data used.

Dataset	**Period**	**Spatial resolution (lon x lat)**	**Institute**	**Reference**
ERA-Interim	1979-2017	0.75° x 0.75°	ECMWF (Europe)	Dee et al. (2011)
HadGEM2-ES	1981-2005 (historical) and 2006-2099 (RCP8.5)	1.87° × 1.25°	MOHC (UK)	Jones et al. (2011)
ACCESS1-3	1979-2005 (historical) and 2006-2100 (RCP8.5)		CAWCR (Australia)	Collier & Uhe (2012)
BCC-CSM1-1M		1.12° x 1.12°	BCC (China)	Wu et al. (2014)
CanESM2		2.81° x 2.79°	CCCma (Canada)	Chylek et al. (2011)
CNRM-CM5		1.40° x 1.40°	CNRM (France)	Voldoire et al. (2013)
GFDL-CM3		2.5° x 2°	GFDL (USA)	Gries et al. (2011)
IPSL-CM5A-MR		2.5° x 1.26°	IPSL (France)	Dufresne et al. (2013)
IPSL-CM5B-LR		3.75° x 1.89°		
MIROC5		1.40° x 1.40°	CCSR, NIES, JAMSTEC (Japan)	Watanabe et al. (2010)
MPI-ESM-MR		1.87° x 1.86°	MPI (Germany)	Giorgetta et al. (2013)

MRI-ESM1		1.12° x 1.12°	MRI (Japan)	Adachi et al. (2013)
NorESM1-M		2.5° x 1.89°	BCCR, NMI (Norway)	Bentsen et al. (2013)

Table 2. Coefficients of pattern correlation between the regimes from ERAI and each climate model over 1979-2017.

Model	**R1**	**R2**	**R3**	**R4**
Average	0.90	0.86	0.51	0.9
HadGEM2-ES	0.94	0.88	0.27	0.80
ACCESS1-3	0.92	0.84	0.75	0.95
BCC-CSM1-1M	0.93	0.88	0.78	0.93
CanESM2	0.93	0.93	0.58	0.96
CNRM-CM5	0.93	0.86	0.48	0.93
GFDL-CM3	0.92	0.87	0.88	0.91
IPSL-CM5A-MR	0.90	0.87	0.52	0.94
IPSL-CM5B-LR	0.91	0.85	0.65	0.93
MIROC5	0.55	0.67	-0.39	0.82
MPI-ESM-MR	0.96	0.93	0.59	0.83
MRI-ESM1	0.91	0.86	0.75	0.81
NorESM1-M	0.95	0.92	0.31	0.94

Figures

Figure 1. Composite maps of the four regimes (one per row) for ERAI (first column) and climate models (second column; each map shows the average of 12 composite maps; third column shows standard deviation of Z500 between the 12 composites). The maps are calculated by averaging the seasonal anomalies (shading) and raw values (contour lines) over the days belonging to the regime. Seasonal anomalies correspond to the raw values minus the average seasonal cycle. The number of days per regime is shown above each map (average of 12 values for the climate models).

Figure 2. Average annual cycle of the frequencies of occurrences for the four regimes of ERAI and the 12 climate models, over 1979-2017. Monthly frequencies correspond to the number of days of regime occurrence divided by the number of days in the month.

Figure 3. As in Fig. 1 but for TAS conditionally to each regime.

Figure 4. Same as Fig. 1 but for the climate models (without ERAI) and seven regimes over 1979-2100. The seasonal anomalies are calculated with reference to the average seasonal cycle of the subperiod (1979-2008, 2071-2100).

Figure 5. As in Fig. 4 but for TAS anomalies conditionally to the regimes.

Figure 6. Average annual cycle of the seven regimes for the 12 climate models in the past (1979-2008) and future (2071-2100).

Figure 7. Frequency of the regimes per year in December, January and February for the 12 climate models.

Figure 8. As in Fig. 7 but for June, July and August.

Figure 9. As in Fig. 6 but after detrending the data from climate models.

Figure 10. As in Fig. 4 but after detrending the data from climate models.

Figure 11. As in Fig. 5 but after detrending the data from climate models.

ERAI 1979–2017

Models 1979–2017

Intermodel variability

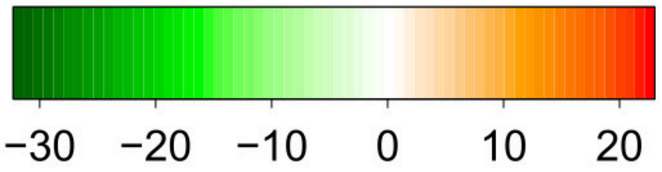

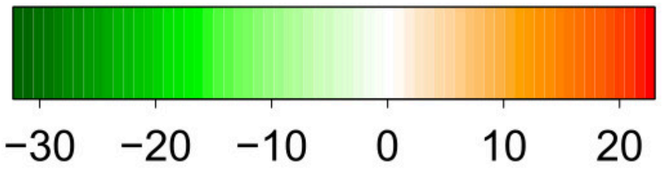

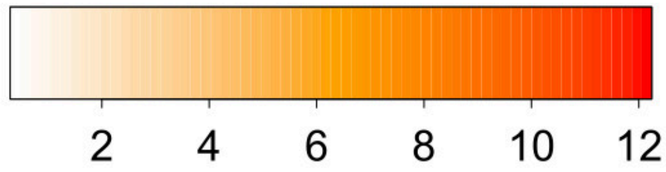

Average Z500 anomaly (m)

Multimodel average Z500 anomaly (m)

Multimodel SD of Z500 anomaly (m)

R1

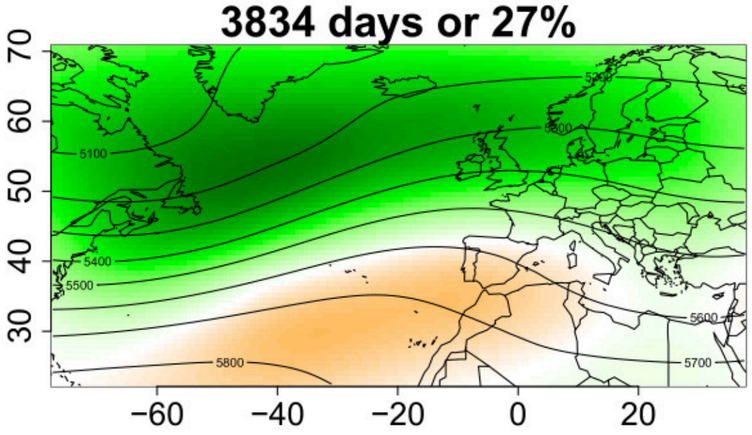

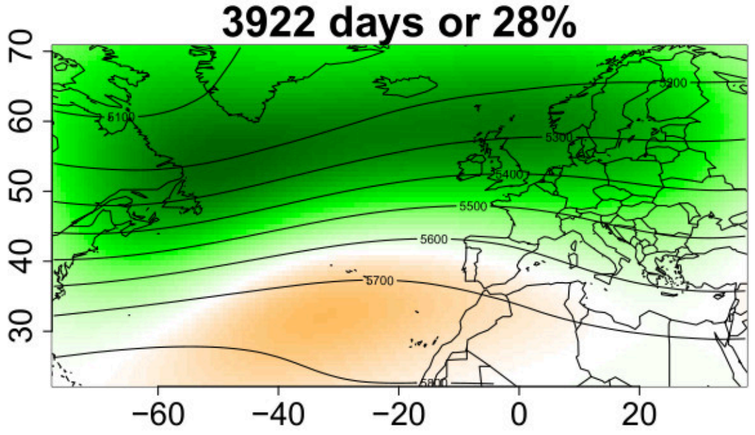

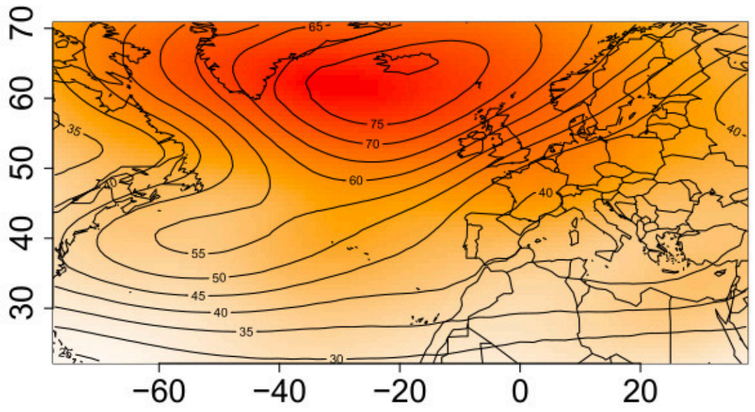

R2

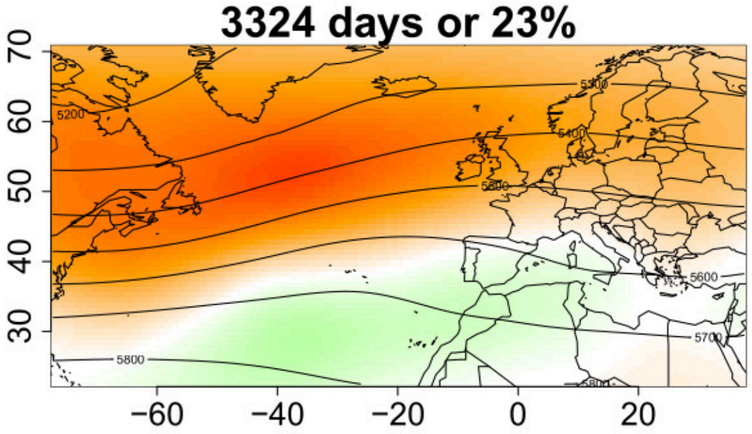

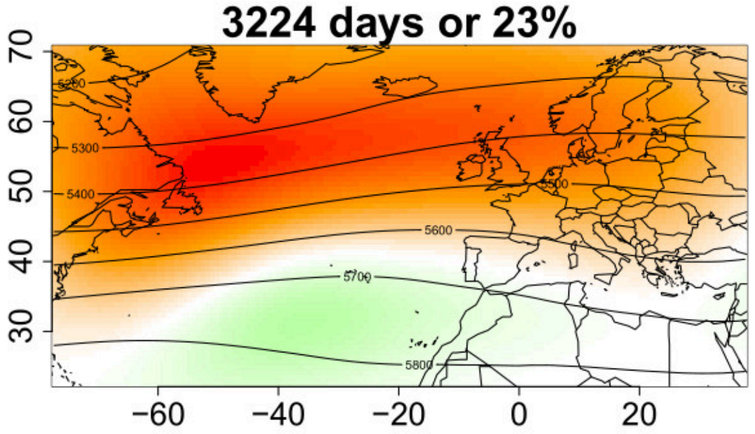

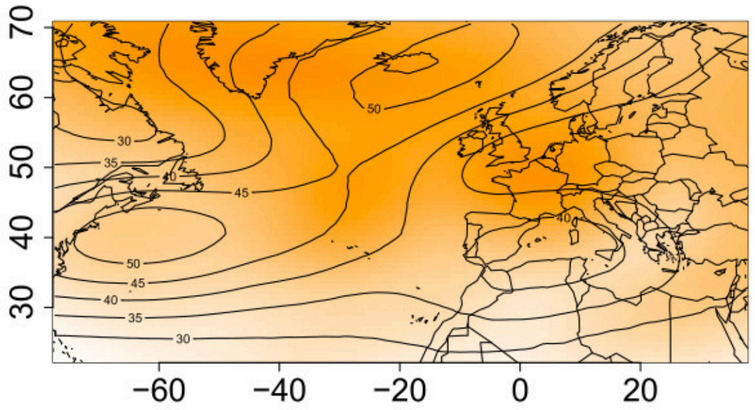

R3

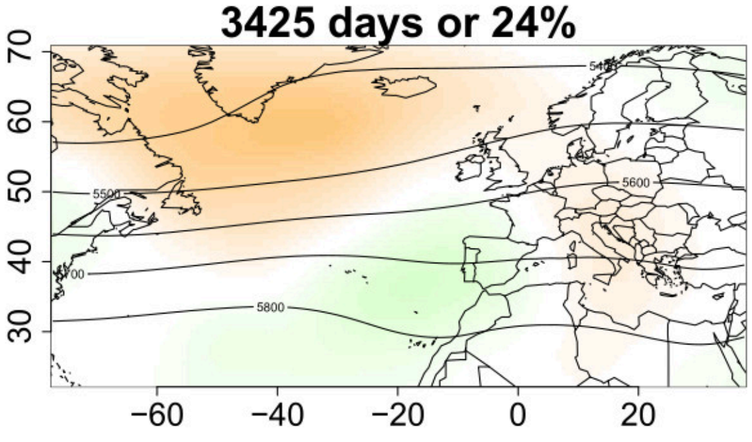

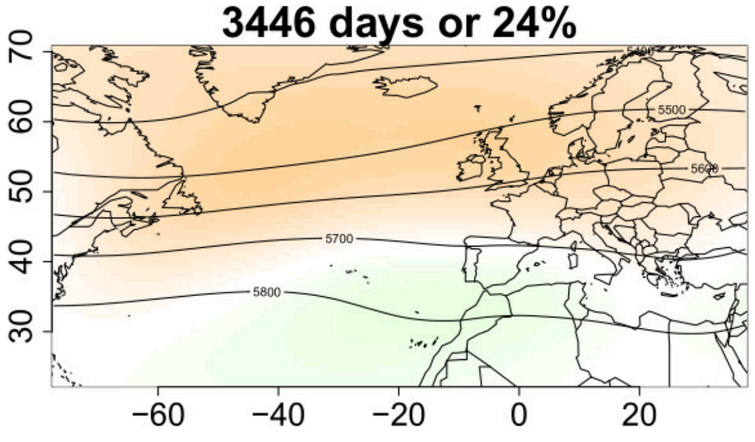

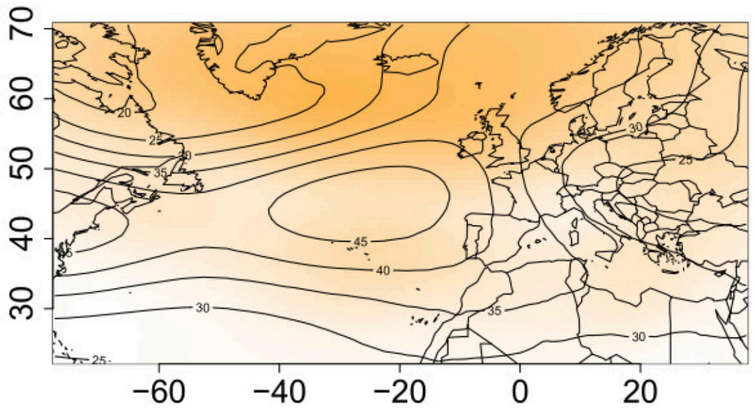

R4

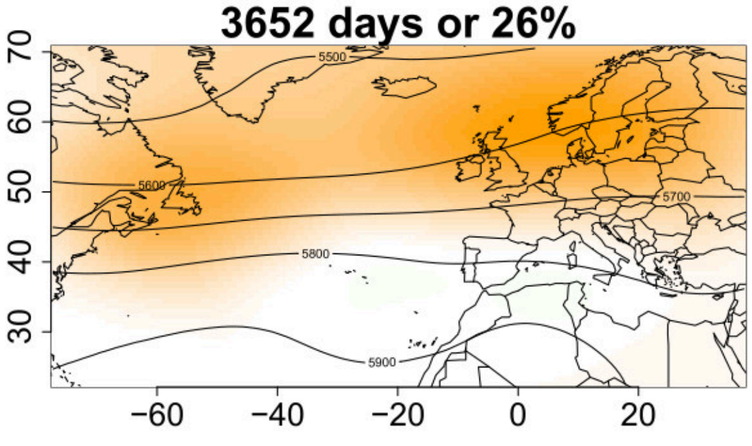

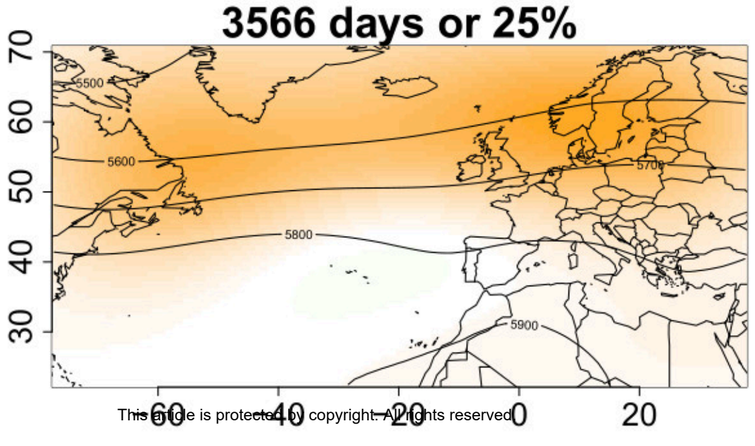

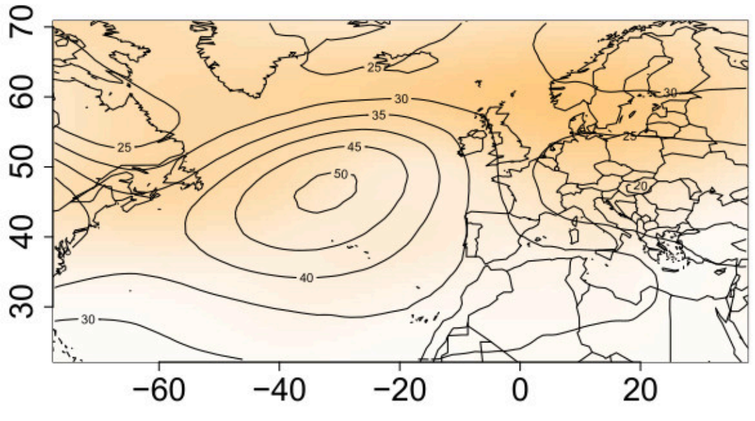

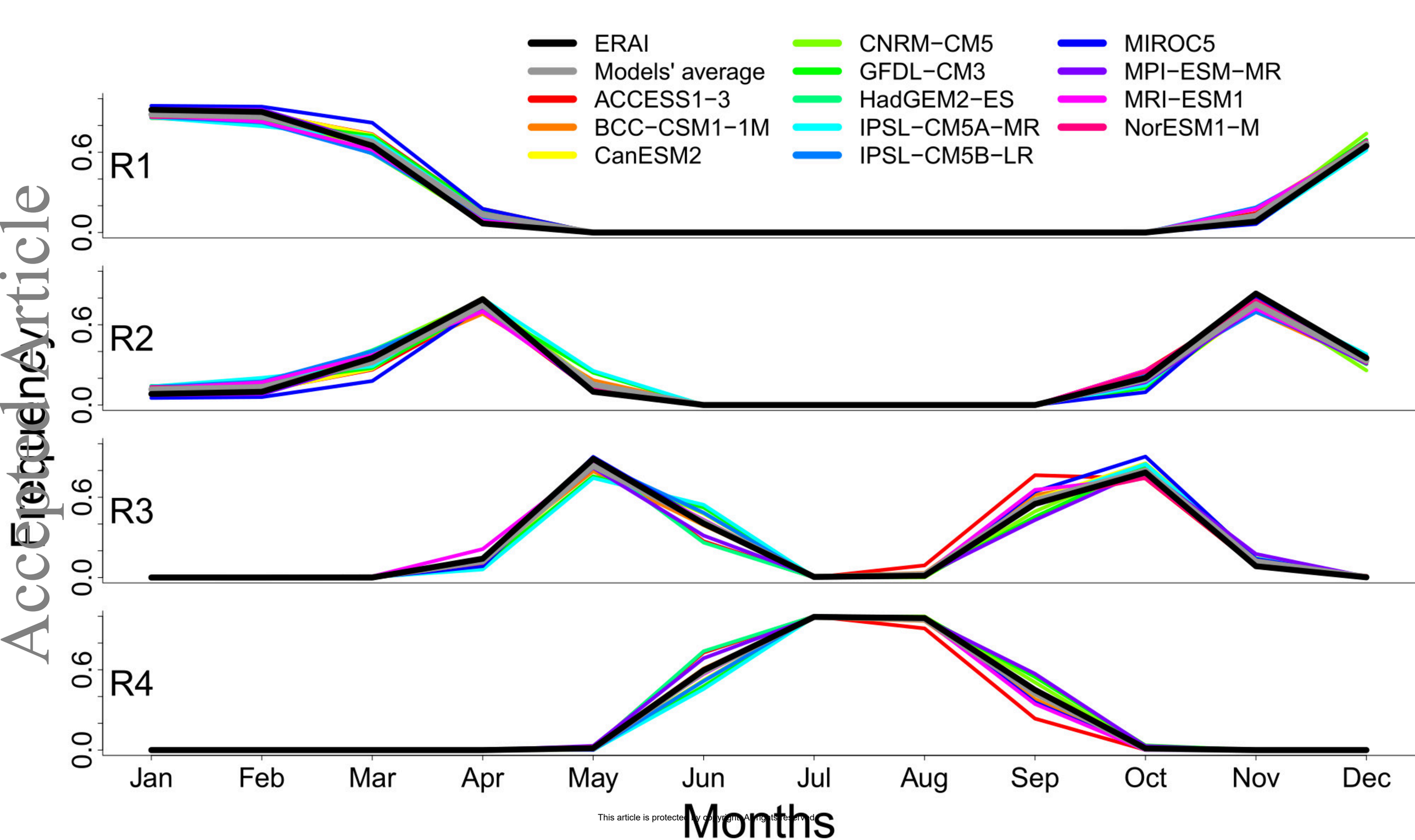

ERAI 1979−2017

Models 1979−2017

Intermodel variability

−0.5 0.0 0.5

−0.5 0.0 0.5

0.1 0.2 0.3 0.4

Average TAS anomaly (°C)

Multimodel average TAS anomaly (°C)

Multimodel SD of TAS anomaly (°C)

R1

3834 days or 27%

3922 days or 28%

R2

3324 days or 23%

3224 days or 23%

R3

3425 days or 24%

3446 days or 24%

R4

3652 days or 26%

3566 days or 25%

Multimodel mean

1979−2008

−150 −50 0 50 100

Average Z500 anomaly (m)

2071−2100

−150 −50 0 50 100

Average Z500 anomaly (m)

Multimodel spread

1979−2008

20 40 60 80

Standard deviation (m)

2071−2100

20 40 60 80

Standard deviation (m)

	1979−2008	2071−2100	1979−2008	2071−2100
R1	2297 days or 21%	103 days or 1%		
R2	2230 days or 21%	1284 days or 12%		
R3	1327 days or 12%	2180 days or 20%		
R4	1291 days or 12%	1673 days or 15%		
R5	1635 days or 15%	1343 days or 12%		
R6	2044 days or 19%	1693 days or 16%		
R7	54 days or <1%	2631 days or 24%		

Multimodel mean

1979−2008

−3 −1 0 1 2 3

Average TAS anomaly (°C)

2071−2100

−3 −1 0 1 2 3

Average TAS anomaly (°C)

Multimodel spread

1979−2008

0.5 1.5 2.5 3.5

Standard deviation (°C)

2071−2100

0.5 1.5 2.5 3.5

Standard deviation (°C)

R1

2297 days or 21%

103 days or 1%

R2

2230 days or 21%

1284 days or 12%

R3

1327 days or 12%

2180 days or 20%

R4

1291 days or 12%

1673 days or 15%

R5

1635 days or 15%

1343 days or 12%

R6

2044 days or 19%

1693 days or 16%

R7

54 days or <1%

2631 days or 24%

Past (1979−2008)
Future (2071−2100)

Models' average
ACCESS1−3
BCC−CSM1−1M
CanESM2
CNRM−CM5
GFDL−CM3
HadGEM2−ES
IPSL−CM5A−MR
IPSL−CM5B−LR
MIROC5
MPI−ESM−MR
MRI−ESM1
NorESM1−M

R1
R2
R3
R4
R5
R6
R7

0
0.8

Jan
Feb
Mar
Apr
May
Jun
Jul
Aug
Sep
Oct
Nov
Dec

Months

Average of models
Envelope of models
R1
R2
R3
R4
R5
R6
R7

December
January
February

0
0.4
0.8

1980
1990
2000
2010
2020
2030
2040
2050
2060
2070
2080
2090
2100

Years

Average of models
Envelope of models
R1
R2
R3
R4
R5
R6
R7

June
July
August
0
0.4
0.8
1980
1990
2000
2010
2020
2030
2040
2050
2060
2070
2080
2090
2100
Years

Past (1979–2008)
Future (2071–2100)
ERAI
Detrended models' average
ACCESS1–3 detrended
BCC–CSM1–1M detrended
CanESM2 detrended
CNRM–CM5 detrended
GFDL–CM3 detrended
HadGEM2–ES detrended
IPSL–CM5A–MR detrended
IPSL–CM5B–LR detrended
MIROC5 detrended
MPI–ESM–MR detrended
MRI–ESM1 detrended
NorESM1–M detrended

R1
R2
R3
R4
R5
R6
R7

0
0.8

Jan Feb Mar Apr May Jun Jul Aug Sep Oct Nov Dec

Months

Multimodel (detrended) mean

1979−2008

−60 −40 −20 0 20

Average Z500 anomaly (m)

2071−2100

−60 −40 −20 0 20

Average Z500 anomaly (m)

Multimodel (detrended) spread

1979−2008

5 10 15 20 25

Standard deviation (m)

2071−2100

5 10 15 20 25

Standard deviation (m)

R1

1487 days or 14%

1484 days or 14%

R2

1648 days or 15%

1644 days or 15%

R3

1541 days or 14%

1548 days or 14%

R4

1537 days or 14%

1540 days or 14%

R5

1502 days or 14%

1508 days or 14%

R6

1422 days or 13%

1394 days or 13%

R7

1740 days or 16%

1790 days or 16%

Multimodel (detrended) mean

1979−2008

−3 −1 0 1 2 3

Average TAS anomaly (°C)

2071−2100

−3 −1 0 1 2 3

Average TAS anomaly (°C)

Multimodel (detrended) spread

1979−2008

1 2 3

Standard deviation (°C)

2071−2100

1 2 3

Standard deviation (°C)

R1

1487 days or 14%

1484 days or 14%

R2

1648 days or 15%

1644 days or 15%

R3

1541 days or 14%

1548 days or 14%

R4

1537 days or 14%

1540 days or 14%

R5

1502 days or 14%

1508 days or 14%

R6

1422 days or 13%

1394 days or 13%

R7

1740 days or 16%

1790 days or 16%

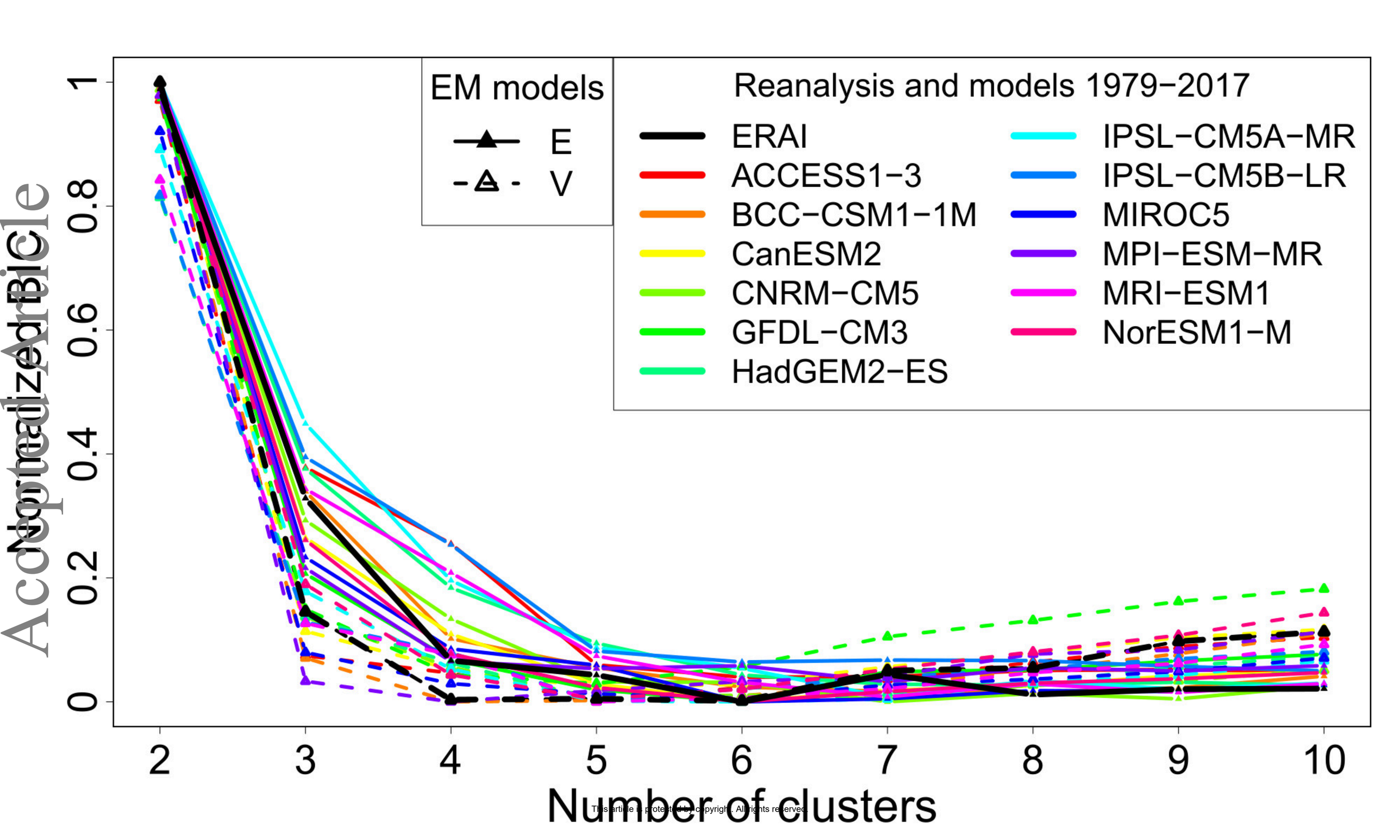

Appendix

Density estimation via Gaussian Mixture Model

Gaussian distributions are ellipsoids in space determined by the mean (location) and covariance matrix (geometric features: volume, shape, orientation). The parameters of the Gaussian Mixture Model (GMM) are the means μ_k , covariance matrix Σ_k , and mixture ratio π_k , describing the K *(k = 1, ..., K)* Gaussian distributions. The estimation of the GMM parameters is done iteratively in the Expectation Maximization (EM) algorithm by maximizing the likelihood that the current statistical model represents the observed data (Fraley & Raftery (2002)). Before being optimized, the GMM parameters are initialized by the result of a hierarchical model-based agglomerative clustering (multivariate), or by separation in quantiles (univariate), rather than random initialization. This approach avoids poor initial partitioning leading to the convergence of the likelihood function to a local maximum rather than a global one (e.g. Scrucca & Raftery (2015)). The principle of EM is based on the possibility to calculate π when knowing α (μ and Σ) and vice versa, thus enabling the optimization of both. After the initialization, the Expectation-step (or E-step) estimates the posterior probability p_{ik} (update of π_{ik}) that the observation $x_i$belongs to f_k with the current parameter estimates (at stage t):

$$p_{ik}^{t} = \frac{\pi_K^t \, f_k \, (\, x_i \, , \alpha_k^t \,)}{\Sigma_{k=1}^{K} \, \pi_K^t \, f_k \, (\, x_i \, , \alpha_k^t \,)}$$

Then, the Maximization-step (or M-step) uses the posterior probabilities to improve the estimates of GMM parameters (stage t + 1):

$$\pi_k^{t+1} = \frac{1}{n} \sum_{i=1}^{n} p_{ik}^{t}$$

$$\mu_k^{t+1} = \frac{1}{n \, \pi_k^{t+1}} \sum_{i=1}^{n} x_i \, p_{ik}^{t}$$

$$\Sigma_k^{t+1} = \frac{1}{n\ \pi_k^{t+1}}\ p_{ik}^t\ (\ x_i - \mu_k^{t+1}\ )'\ (\ x_i - \mu_k^{t+1}\ )$$

where n is the number of observations. The algorithm repeats the E- and M-steps iteratively until termination when model parameters converge and the maximum likelihood is reached (convergence of the log-likelihood function) or after a maximum number of iterations.

Model selection with the BIC and covariance matrix

The Bayesian Information Criterion (BIC) is a criterion for model selection that helps to prevent overfitting by introducing penalty terms for the complexity of the model (number of parameters). In the calculation of the BIC, these penalty terms compete with the likelihood function which determines whether adding parameters improves the model by better fitting the observed data. In our case, minimizing the BIC achieves a good compromise between keeping the model simple and a good representation of the observed data.

$$BIC\ (K) = p\ log(n) - 2\ log(L)$$

where K is the number of clusters, L the likelihood of the parameterized mixture model, p the number of parameters to estimate, and n the size of the sample (e.g. 14235 days over 1979-2017). An additional constraint on the definition of clusters is on the covariance matrix. Our GMM is univariate (since we only use PC1) so the variance can be equal (E model) or different (V model) between clusters (i.e. constraint on volume but not on shape or orientation of clusters).

Figure A1. Bayesian information criterion (BIC) of the clustering models in function of the number of clusters and model type for ERAI and each climate model over 1979-2017 (exception of HadGEM2-ES: 1981-2017). The BIC values are normalized between 0 (best EM model) and 1 (worst EM model). E: equal variance, V: variable variance.

Regime conditional trends

The maps of linear trends by regime are obtained by using multiple linear regressions. At each gridpoint, the model of multiple linear regression estimates the contribution of each regime (k = *1, ..., K*) to the evolution of the variable (Z500 or TAS):

$$y_t = \alpha_0 + \left[\ \sum_{k=1}^{K} \mathbb{1}_{t,k}\ (\ \alpha_k + \beta_k\ t\ )\ \right] + \varepsilon_t$$

with

$$\alpha_1 = 0$$

and

$$\mathbb{1}_{t,k} = 0, if\ regime\ \neq k\ at\ time\ t$$

$$\mathbb{1}_{t,k} = 1, if\ regime\ = k\ at\ time\ t$$

where y_t is the value of the daily variable, α_0 is the general intercept of the multiple regression model, $1_{t,k}$ is the conditional attribution of days per regime, $\alpha_k$is the intercept of the regression per regime, β_k is the slope of the regression per regime, t is time, and ε is the error. The intercept of the regression for regime 1 is used as the general intercept (α_0) of the multiple regression model. The intercept (α_k) of the regression for each regime (k = *1, ..., K*) is the intercept difference with α_0, this difference being 0 for regime 1 (α_1). The multiple linear regression estimates the parameters (intercepts, slopes) while taking into account the temporality of the regimes (non-continuous), and while minimizing the error (residual sum of squares). The decadal trends are obtained by multiplying the regression slope per regime by the number of days per decade (3600 in the Hadley Center model and 3650 in the 11 other models).

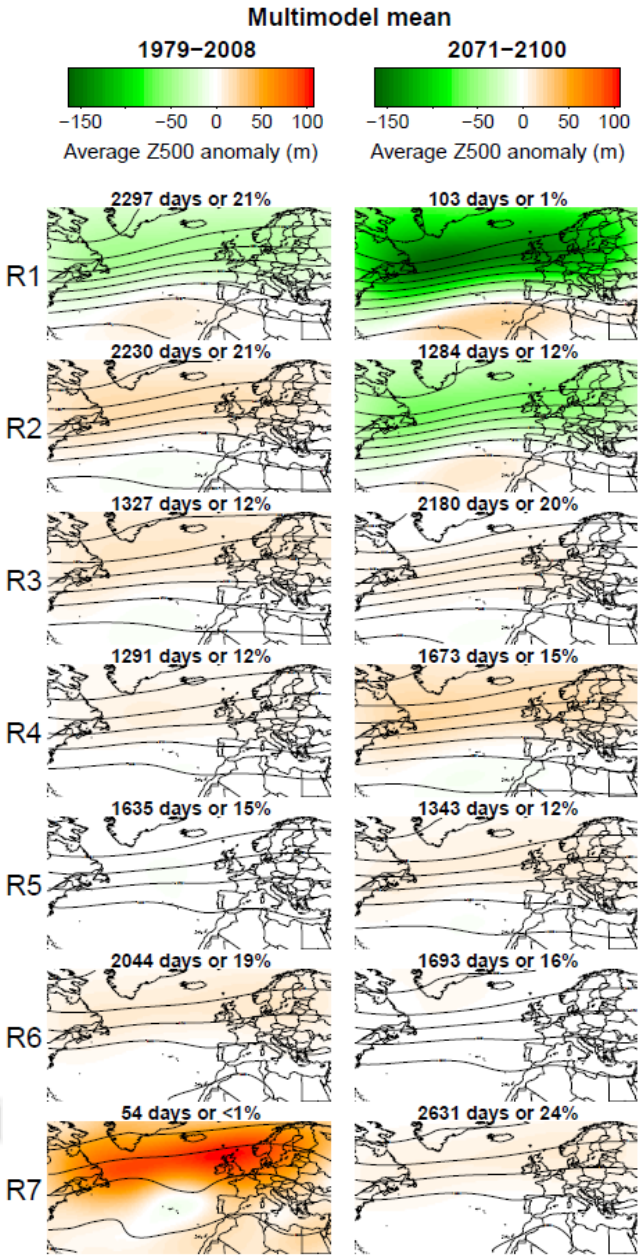

Seasonal circulation regimes in the North Atlantic: towards a new seasonality

F. Breton, M. Vrac, P. Yiou, P. Vaittinada Ayar, A. Jézéquel*

Understanding future changes in atmospheric seasonality is essential for human and natural systems. We use geopotential height and surface temperature from a reanalysis and 12 climate models, to find that historical winter conditions happen less while historical summer conditions happen more. However, seasonal structures remain similar (spatial pattern, time of occurrence) relatively to the year-round increase of geopotential height and surface temperature.